Astron. Astrophys. 343, 241–250 (1999)

ASTRONOMY AND ASTROPHYSICS

Dynamics of the circumstellar envelope of RT Virginis on the basis of the H_2O maser monitoring

E.E. Lekht[1], **J.E. Mendoza-Torres**[1], **M.I. Pashchenko**[2], **and I.I. Berulis**[3,4]

[1] Instituto Nacional de Astrofísica, Óptica y Electrónica, Luis Enrique Erro No. 1, Apdo Postal 51 y 216, 72840 Tonantzintla, Puebla, México
[2] Sternberg Astronomical Institute, 13 Universitetskij prospekt, 119899 Moscow, Russia
[3] Pushchino Radio Astronomy Observatory, Astrospace Centre, Lebedev Institute of Physics, Russian Academy of Sciences, 142292 Pushchino, Russia
[4] Technological University, Kaunas, Lithuania

Received 27 May 1998 / Accepted 3 November 1998

Abstract. This paper continues the earlier work (Mendoza–Torres et al. 1997) on single-dish 22-GHz observations of the H_2O maser associated with the semiregular variable (SRb-type) RT Vir. New spectra, obtained in 1996–1998, are presented, and an analysis of the emission of individual spectral features during the interval of 1986–1998 is performed. All the observations have been carried out on the RT–22 radio telescope of the Pushchino Radio Astronomy Observatory, Lebedev Institute of Physics, Russian Academy of Sciences. As a result of long-term monitoring, the character of variability of multiple spectral components was traced in detail. For many features, a drift in radial velocity was found. There are time intervals with preferential drift direction of the majority of the spectral features. This trend was the most pronounced at velocities <15.5 km s^{-1}. Possible causes of the drift observed are discussed. From a superposition of all the spectra and from the mean spectrum for 1984–1998, stellar velocity V_* was determined. It is estimated as 17.3 ± 0.2 km s^{-1}. The time interval from March to June 1998 is considered as the period of maximum activity of the H_2O maser RT Vir during the entire timespan of its observations.

Key words: masers – stars: circumstellar matter – stars: individual: RT Vir – radio lines: stars

1. Introduction

The dynamics of the envelope of a late-type star can be explained in the framework of the expanding shell model. According to interferometric observations (e.g., Reid & Menten 1990; Yates & Cohen 1994), maser condensations, localized within the envelopes of some late–type stars, undoubtedly show radial motions. However, the standard expanding shell model is incapable to explain some observations of the maser emission from semiregular variable stars. For instance, Bowers & Johnston (1994) note considerable asymmetry in the angular distribution of the H_2O maser features with respect to the stellar positions. This effect is most conspicuous in the H_2O maser RT Vir.

Send offprint requests to: J.E. Mendoza-Torres

The H_2O 22–GHz spectra of RT Vir have displayed a strong time variability (Mendoza–Torres et al. 1997). Similar temporal variations were observed also in the H_2O line at 325 GHz (Yates & Cohen 1996). In addition, maser emission in other molecular lines was observed: SiO (Spencer et al. 1981) and OH (Le Squeren et al. 1970); their variability is considerable, too.

The variability of the total flux of the H_2O line in RT Vir is very complicated (Berulis et al. 1987). The data analysis is difficult because it seems impossible to reveal the H_2O emission variation that would correlate with the visual brightness variability. Furthermore, the data on the visual light curve of RT Vir are insufficient. In the case of Miras, observations have shown that the H_2O flux variations follow (with a delay of 0.1–0.2P) the visual light curve (Nyman et al. 1986). For U Ori the delay is changing with a superperiod of about 12 years (Berulis et al. 1994). Berulis et al. explain this effect by pulsations of the envelope of U Ori with this superperiod.

VLA observations at 22 GHz toward RT Vir were carried out at epochs 1985.05 (Bowers et al. 1993) and 1988.95 (Bowers & Johnston 1994). The angular distribution of maser spots is complex, this is especially prominent at the latter epoch. A comparison of the two maps shows considerable differences. Nevertheless, it is clear that at both epochs the most intense features lie in the blueshifted part of the spectrum (at velocities of about 12–14 km s^{-1}).

Recently Richards et al. (1998) have undertaken on MERLIN a program of repeated mapping of RT Vir, covering an entire light cycle of the star ($\sim 155^d$). This enabled them to trace the evolution of individual features and to make a movie, showing an indeed complex structure with probably multiple shells. This indicates that the mass loss rate from RT Vir is time–variable.

The most plausible model of the H_2O maser emission region for semiregular variables is an ellipsoidally-shaped shell. In this shell clumps, segments or filaments are distributed over radius, as masering condensations (Bowers & Johnston 1994). According to this model, some clumps of the gas are accelerated to the terminal outflow velocity at distances of $\geq$20 a.u. from the star. In the case of RT Vir, the outflow from the star is slightly bipolar (Richards et al. 1998). Long-term observations

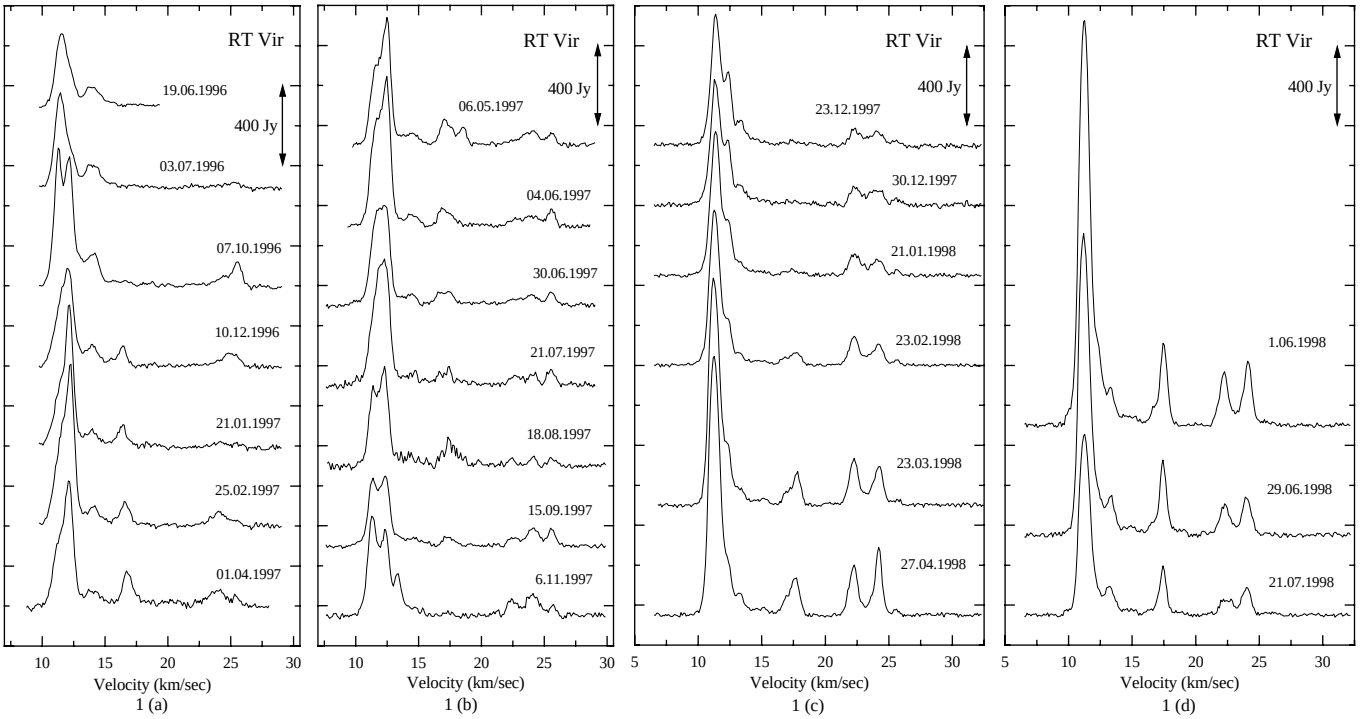

Fig. 1a–d. Spectra of the H_2O maser emission of RT Vir from June 1996 to July 1998. The flux scale, shown by the vertical arrow, is 400 Jy.

of the H_2O maser emission would allow to trace evolution of clumps and filaments in the stellar shell and perhaps variations of the parameters of the shell itself.

The velocity of RT Vir was estimated by Bowers and Johnston (1994). Based on the structure of the OH maser profiles at 1612 MHz, they found a velocity of 17 km s^{-1}. The velocities, estimated from other molecular lines (H_2O, vibrational transitions of SiO and CO) are somewhat different and lie within an interval of -0.7 to $+1.5$ km s^{-1} with respect to 17 km s^{-1}.

This work continues the earlier investigation of the 1.35–cm H_2O maser emission toward the semiregular variable RT Vir, undertaken by Mendoza-Torres et al. (1997). Here we analyze the evolution of individual spectral components. In total we have obtained 99 spectra covering a time interval since the end of 1984 till July 1998. The spectra observed from the end of 1984 to the beginning of 1986 and their analysis were published by Berulis et al. (1987), and those from 1986 to March 1996 – by Mendoza–Torres et al. (1997). All the subsequent spectra (from June 1996 to July 1998) are presented in this paper (Fig. 1a–d).

2. Observations and data reduction

2.1. Observations

The observations were carried out on the RT-22 radio telescope of the Pushchino Radio Astronomy Observatory (Astrospace Center, Lebedev Institute of Physics, Russian Academy of Sciences) in Pushchino, Moscow Region, Russia. As the receiver front end, a liquid-helium-cooled maser amplifier of the 22-GHz band was used, yielding a system noise temperature of 200–300 K. In the observations of 1993–1998, we used a cooled transistor amplifier. The antenna beamwidth at 22 GHz is $2'.6$. The observations were performed by the ON–ON method with a symmetrical beam switching. At first, the antenna was pointed to the source by one feed horn and then by the other. During the former stage, a calibration signal from a noise tube was injected for some time. Tuning to the receiving frequency of the 22.235-GHz H_2O line was done with an account for the Doppler shift, caused by the orbital motion and rotation of the Earth. For spectral analysis, we used a 96-channel, and starting from mid-1997 a 128-channel filter bank with a frequency resolution of 7.5 kHz (101 m s^{-1} in radial velocity at the frequency of the 1.35-cm H_2O line). The necessary frequency band was covered by retuning the frequency of the local oscillator.

To achieve a sufficient sensitivity, the integration time for each spectrum was about 15 minutes. An antenna temperature of 1 K for a nonpolarized source corresponds to a flux density of 25 Jy. The data reduction consisted in establishing the radial-velocity scale of the spectra, subtraction of baselines, accounting for absorption in the Earth's atmosphere, averaging and smoothing of the spectra. The mean interval between two consecutive observing sessions was 1.65 months.

2.2. Data reduction

For observations in the H_2O line, accounting for absorption of radio waves by atmospheric water vapour and molecular oxygen is of primary importance. We calculated the atmospheric absorption by the method, presented by Zhevakin & Naumov (1963) and Tseitlin (1976). We adopted a plane-parallel model of the terrestrial atmosphere, which is acceptable for observations of the sources at elevations $h > 5^\circ$. In this model, the

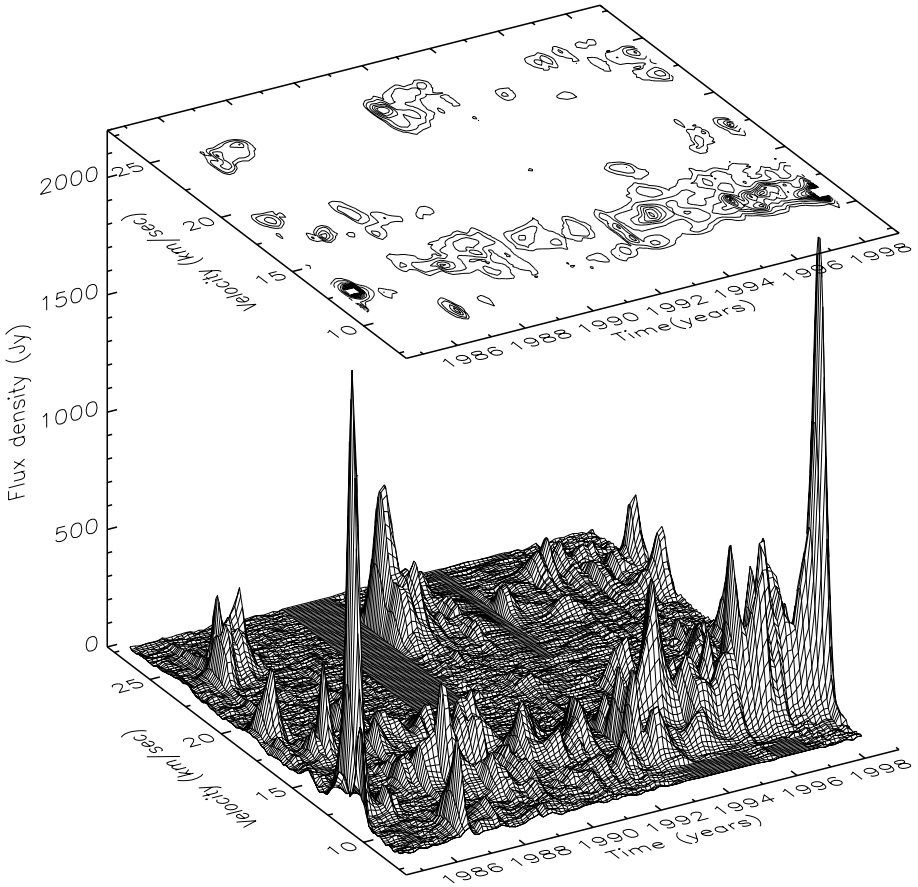

Fig. 2. Three–dimensional (3D) representation of the 22.2-GHz H_2O maser emission of RT Vir.

relationship between the observed antenna temperature (T_{Aobs}) and the true one, corrected for absorption (T_{A0}), is

$$T_{A0} = T_{Aobs} \exp(\kappa \csc h), \quad (1)$$

where κ is the optical depth of the Earth atmosphere at the zenith:

$$\kappa = 0.02 \left(\frac{p}{760}\right)^2 \left(\frac{288}{T}\right)^{5/2} + 0.0107\rho \cdot \frac{760}{p} \left(\frac{288}{T}\right)^2, \quad (2)$$

p is atmospheric pressure (mm mercury column), T is air temperature (K) and ρ is absolute humidity (g/m^3) in the surface boundary layer. In (2), the first term in the right-hand side describes the absorption by molecular oxygen (O_2), and the second – the water-vapour absorption. During our observations, we recorded relative humidity $r = \frac{e}{E} \cdot 100\%$, where e is water-vapour pressure (mb), E is pressure of saturated vapour for given temperature T (Matveev 1976):

$$\lg E = 26.25102 - \frac{3049.50}{T} - 5.86970 \cdot \lg T. \quad (3)$$

Absolute humidity ρ was calculated as

$$\rho = \frac{220e}{T}. \quad (4)$$

We usually observed RT Vir at elevations $35^\circ < h < 50^\circ$. Depending on weather conditions, coefficient κ varied in the limits of 0.03–0.15. In this case, the correction for absorption was from 5 to 25%. Only under the most unfavourable conditions (T ∼300 K, ρ ∼80–90%), κ was as high as 0.20–0.25, and the correction for absorption ∼50%.

3. Presentation of the data

The results of the observations are presented in Fig. 1a–d in the form of spectral profiles of the H_2O line. The vertical-axis scale is in units of flux density F_ν (Janskys). The horizontal axis displays radial velocities, referred to the Local Standard of Rest ($V_{\rm LSR}$).

3.1. Three-dimensional data presentation

Fig. 2 shows the three-dimensional (3D) presentation of the H_2O maser-emission spectra of RT Vir, including all the profiles obtained since the end of 1984. To construct a 3D image, it is necessary to have a regular grid in the velocity–time plane. The velocity intervals between two neighbouring filter-bank channels are equal along the entire spectrum. However, time intervals between two consecutive observations are, in the majority of cases, different. Therefore, the observational data are unevenly spread over the temporal axis. We calculated the equivalent intermediate values on the temporal axis, using the IDL triangulation procedure. These values determined, we computed the fluxes for the new grid by the method of linear interpolation, using the

Trigrid IDL procedure. In the upper plane of Fig. 2, we present the isophotes of the H_2O maser emission, i.e. the level lines of equal fluxes. The contour interval is 100 Jy.

As a result, Fig. 2 can give us a good idea about the evolution of the maser emission throughout the entire observational interval. The maser emission of individual components displays short-term bursts. The mean duration of a burst at the half-maximum level is about 0.5 yr. None of the features remained stable. An exception may be the interval since 1996, when an emission feature at 11.4 km s^{-1}, relatively stable in velocity, though strongly flux-variable, was observed. Beginning from 1996, the H_2O maser in RT Vir has displayed the strongest activity during the entire timespan of its observations.

3.2. Gaussian fitting

Each spectrum observed was presented as a superposition of gaussian curves. The aim was to determine the peak flux, radial velocity and half-maximum width of each gaussian. Initially, we set the position, amplitude and width of the main (reference) features, namely of those, for which the flux maxima in the spectra obtained were sufficiently conspicuous. After subtracting them from the raw spectrum, we got the residual curve. The rest gaussians were fitted to the residual curve. We set their number and approximate parameters. Then, using a dedicated software based on least-square-fitting, we calculated refined values of the gaussian parameters. Sometimes, for the most complex spectra, we repeated this procedure several times, until the residual curve sank within the limits of the noise level.

The test for this method was a comparison of the current-spectrum gaussians with those of the previous and next spectra. To evaluate the quality of the gaussian fitting method, we used the following criteria.

1. Absence of velocity discontinuities in two consecutive spectra. If no regular drift is present, the velocity spectra should not exceed ± 0.1 km s^{-1} (for the features that are more or less isolated in the spectrum, or for the features with pronounced peaks) and ± 0.2 for the rest features. If a velocity drift was present, we measured the deviations with respect to the fitted curve.
2. Absence of strong linewidth variations.
3. Restrictions on the linewidth $(0.5 < \delta V < 1.1$ km s$^{-1})$.
4. Absence of strong jumps of the flux density.

In the case, where a weak component lies in the wing of a much stronger component, an increased error is possible, especially in the determination of its velocity.

In total, we detected 66 spectral components (39 at $V_{\rm LSR} < 15.5$ km s^{-1} and 27 at $V_{\rm LSR} > 21$ km s^{-1}) that satisfied our criteria. The rest features were visible in not more than two consecutive spectra, or their velocity scatter from one spectrum to another was sufficiently broad, so we could not identify them as the same spectral feature.

Table 1 lists the data for 22 most durable components at $V_{\rm LSR} < 15.5$ km s^{-1}. The numbers of the components correspond to those in Figs. 3 and 4. The majority of the components have a velocity drift; therefore, the velocities at the beginning and end of the component evolution are given. Feature 10 has a complex character of the drift; for it, the maximum and minimum velocities are given. Column 3 lists the minimum linewidths and linewidths during the flux maximum. Some features were heavily blended by other features. For these, the most reliable linewidths were determined near the epoch of maxima of their fluxes. For this reason, only one linewidth is listed for such components. The flux is given for the emission maximum of each component. The timespan, during which we observed the given component, is listed in column 5.

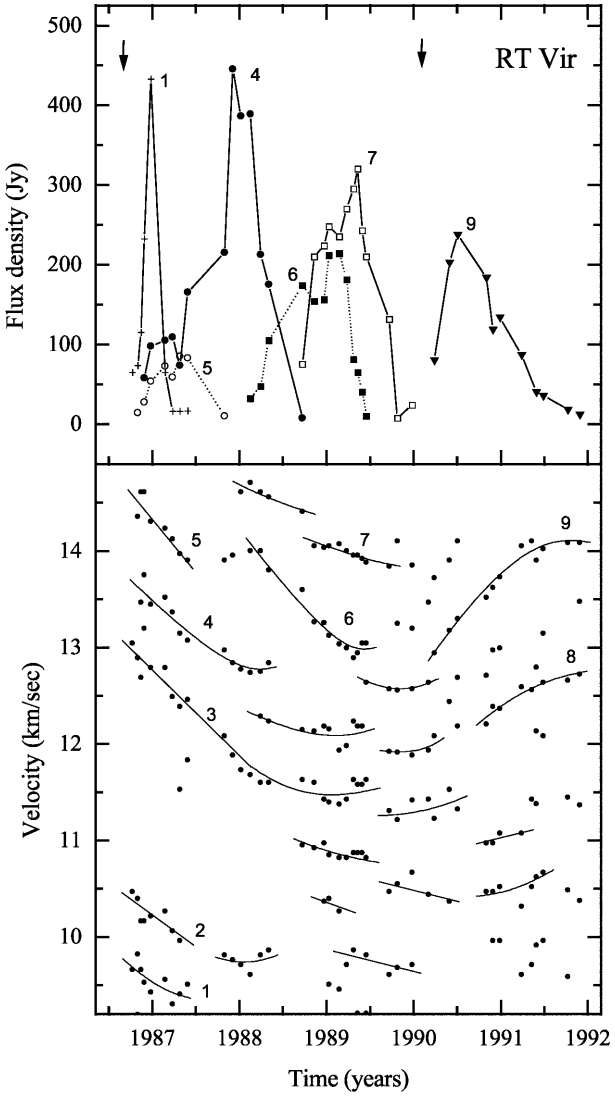

Fig. 3. Variability of flux and velocity of the main features at $V_{\rm LSR} < 15$ km s^{-1} in 1986–1992. Arrows denote the epochs of the minima of the integral flux.

3.3. Components of the first group

According to Mendoza-Torres et al. (1997), the H_2O maser emission of RT Vir is concentrated within three separate spectral groups. Here, we have analyzed two groups – the first and the

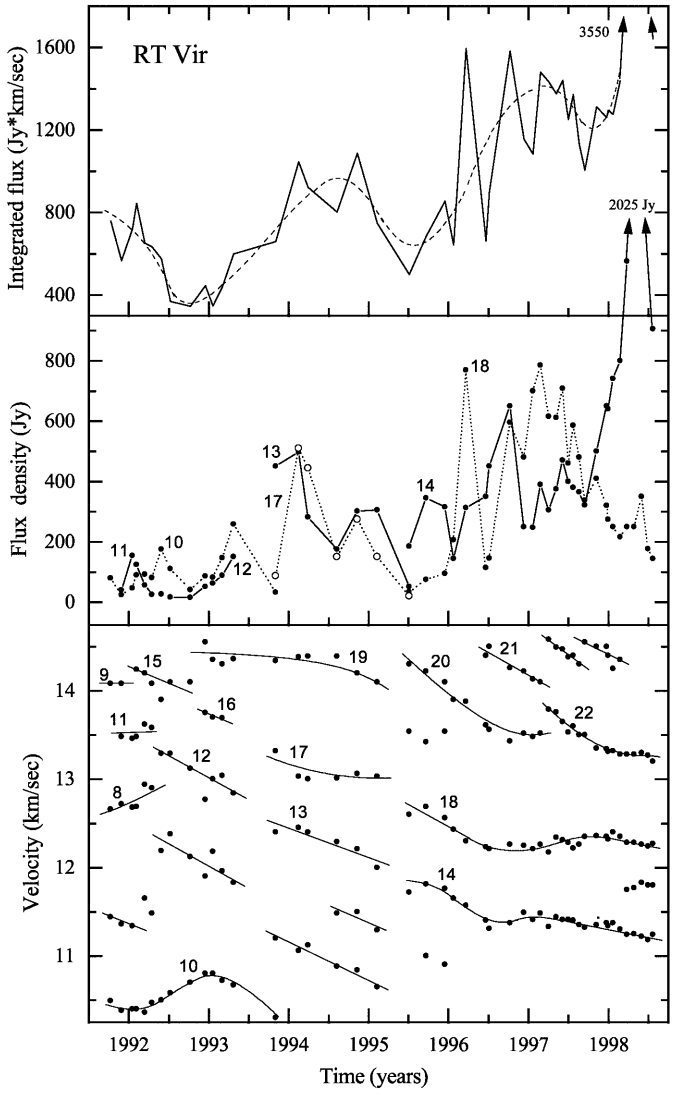

Fig. 4. Same as Fig. 3, but for the time interval of 1991.5–1998.4. In addition, the variability of the integral flux is shown in the upper graph.

third. For the first group of the features, the results are presented in Fig. 3–6. Flux variations of the most intense components for 1986–1992 are given in the upper panel of Fig. 3. The arrows mark the epochs of minimum integral flux. We observe alternating appearance and disappearance of the main components for this time interval. The growth of the flux of features 1, 4, 5 and 7 was slower than their decline. After the minimum of maser activity, which took place at the end of 1990 and beginning of 1991, the character of the flux evolution of component 9 was different: a rapid growth of the flux was followed by a slow decline.

All the gaussians we have fitted are shown in the velocity–time diagram (lower panels of Fig. 3 and 4). The smooth curves are drawn through the points that, according to our criteria, belong to the same features. For convenience of the analysis, the most intense features are labeled with numbers. The majority of the points not connected by curves are most probably identified with faint, short-living features.

Table 1. Parameters of main features of H_2O spectra

N	$V_{\rm LSR}$ (km s^{-1})		δV (km s^{-1})		F (Jy)	τ (Year)
1	9.75	9.35		0.90	430	0.72
2	10.50	9.90		0.65	122	0.66
3	13.05	11.55		0.85	115	2.75
4	13.65	12.75	0.64	0.68	445	1.54
5	14.55	13.90	0.62		80	0.66
6	14.00	13.00	0.72	0.83	210	1.43
7	14.05	13.80	0.76	0.88	320	~ 1
8	12.15	12.90	0.80	1.00	190	1.55
9	12.95	14.07	0.70	0.75	240	1.76
10	10.35	10.75	0.75	0.83	250	2.14
11	13.50	13.60	0.90	0.90	150	0.5
12	13.30	12.80	0.80	1.00	145	1.0
13	12.50	12.00	0.78	0.82	490	1.38
14	11.77	11.25	0.78	0.94	2025	> 3
15	14.22	14.00	~ 1	–	18	0.77
16	13.75	13.65	0.83	–	44	0.33
17	13.25	13.00	0.69	0.82	500	1.38
18	12.70	12.25	0.70	0.76	790	> 3
19	14.50	14.05	0.78		135	2.26
20	14.30	13.50	0.72		320	1.76
21	14.50	14.05	0.80		145	0.82
22	13.80	13.25	0.67	0.72	185	> 1.5

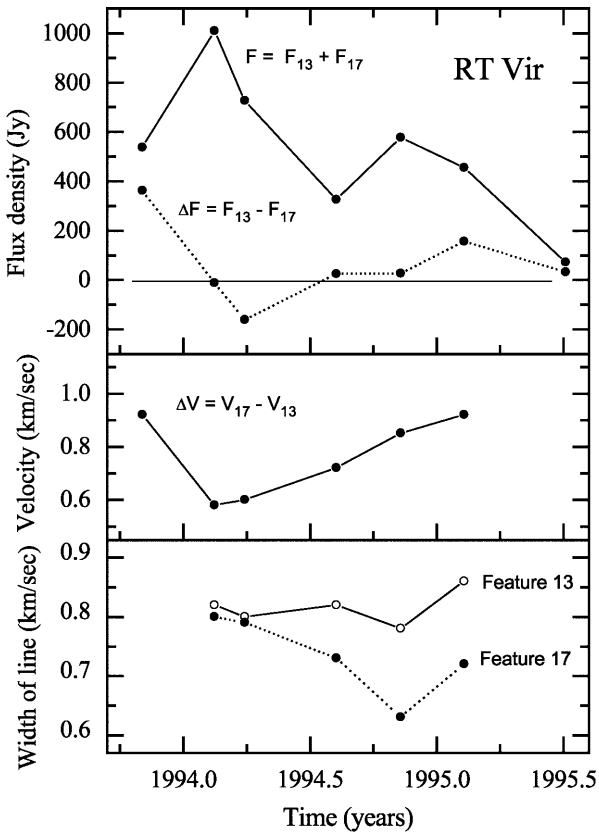

Fig. 5. Variability of the sum and difference of the fluxes for two main spectral features at velocities $V_{\rm LSR} < 15$ km s^{-1}, the differences of their radial velocities and linewidths in 1993.7–1995.5.

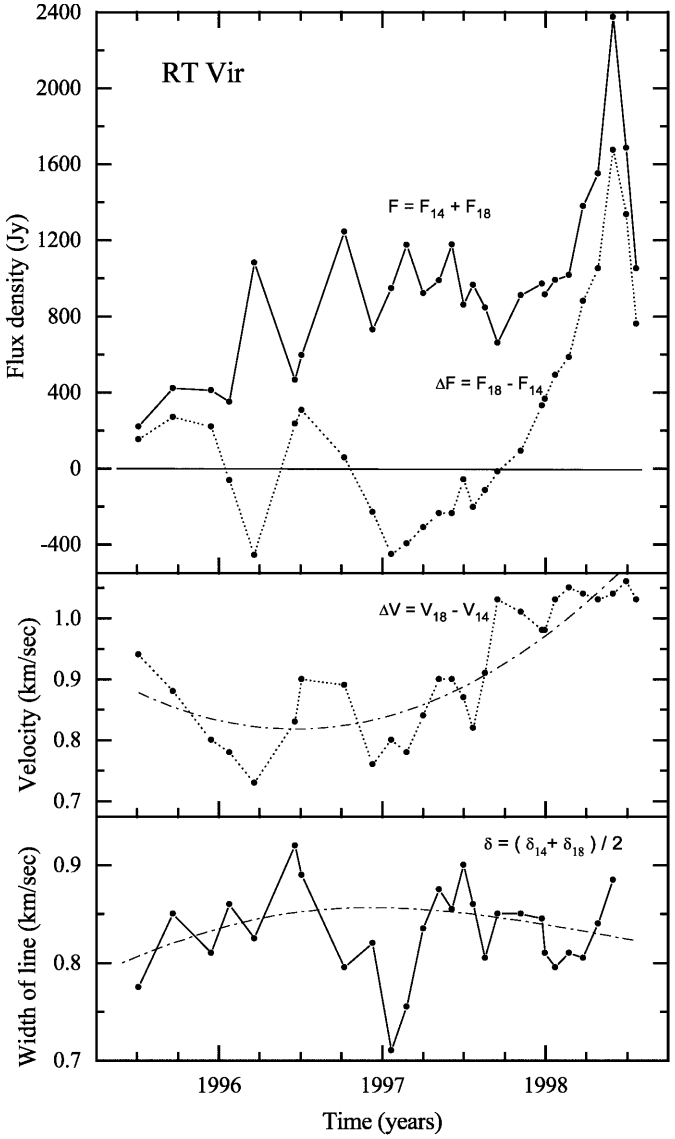

Fig. 6. Variability of sum F and difference ΔF for two main features of the first group, difference of their radial velocities ΔV and mean linewidth δV in 1995.5–1998.3. Dash-and-dot lines show the fitted polynomials.

The evolution of flux (of the strongest features) and of radial velocities of all the features detected from 1992 to July 1998 is presented in Fig. 4. The variations of these parameters are given in comparison with the curve of the total-flux variability, taken from our previous work (Mendoza–Torres et al. 1997). This curve, together with additional data of the subsequent observations, is shown in the upper panel of Fig. 4. In 1998, a strong flare of emission happened at a velocity of 11.2 km s^{-1}; its intensity was only slightly inferior to that of the strongest flare of early 1985 (Berulis et al. 1987).

In Fig. 5, an analysis of the variations of the flux, radial velocity and linewidth for the two strongest features (13 and 17) of 1993.5–1995.5 interval is presented. The sum (F) and difference (ΔF) of fluxes of these features are shown in the upper panel. The middle panel shows the difference of the radial velocities of these features. The behaviour of ΔF is quite similar to that of ΔV. The lower panel shows the linewidth variations.

The results of an analogous analysis for features 14 and 18 (the strongest ones in 1995–1998) are presented in Fig. 6. Again, the upper panel shows the sum ($F = F_{14} + F_{18}$) and difference ($\Delta F = F_{18} - F_{14}$) of the fluxes. In contrast to features 13 and 17, the fluxes of these features anticorrelate. The middle panel shows the velocity difference ($\Delta V = V_{18} - V_{14}$) as well as the fitted polynomial (dot-and-dash line). The same was done for the mean linewidth of these features. Parameters ΔF and ΔV correlate. This means that when the flux difference reaches maximum, the spectral separation of the features is maximum, too.

3.4. Components of the second group

The central group ($15.5 < V_{\rm LSR} < 21$ km s^{-1}) was always the least intense, with the exception of mid-1986, when a flare of a short-living feature at 17 km s^{-1} reached a peak flux density of 380 Jy. For the observer, these features have radial velocities close to the stellar velocity. However, they may have non-radial motions, too (Collison & Fix 1992; Pascoli 1992). For this reason, their behaviour may considerably differ from that of other groups of features. Furthermore, in all the spectra the central group is always separated from the other groups by a pronounced gap, which is obviously not mere chance. The results of investigation of this group of features will be given in our forthcoming paper.

3.5. Components of the third group

For the third group ($V_{\rm LSR} > 21$ km s^{-1}), three intervals of activity were observed. During the first of them (1985–1987), the spectra had two main peaks, separated by approximately 0.6–1 km/s. Feature 1 was the most long-living. Its active phase lasted for about 1.5 yr. Its radial-velocity drift can be fitted by a polynomial with maximum velocity at the end of 1986. The other feature seems to be the result of consecutive brightening of two different components (2 and 3) with similar, however different radial velocities. The velocity drift directions of features 1 and 2, 1 and 3 coincide. During the second and third intervals of activity (1991–1998) of this spectral group, the radial-velocity drift of some components was also observed (Fig. 8 and 9).

3.6. Superposition of all the spectra and the average spectrum

The H_2O spectra of RT Vir change strongly and rapidly. The instantaneous spectrum is formed by the emission from those maser spots in the stellar envelope, where the conditions at the given moment are the most favourable. However, in course of long-term monitoring a great number of eventual maser regions will sooner or later manifest themselves. Therefore, a superposition of all the spectra, rather than a single spectrum, will better reflect the probability of the emission as a function of the velocity with respect to the star. Since our observations have

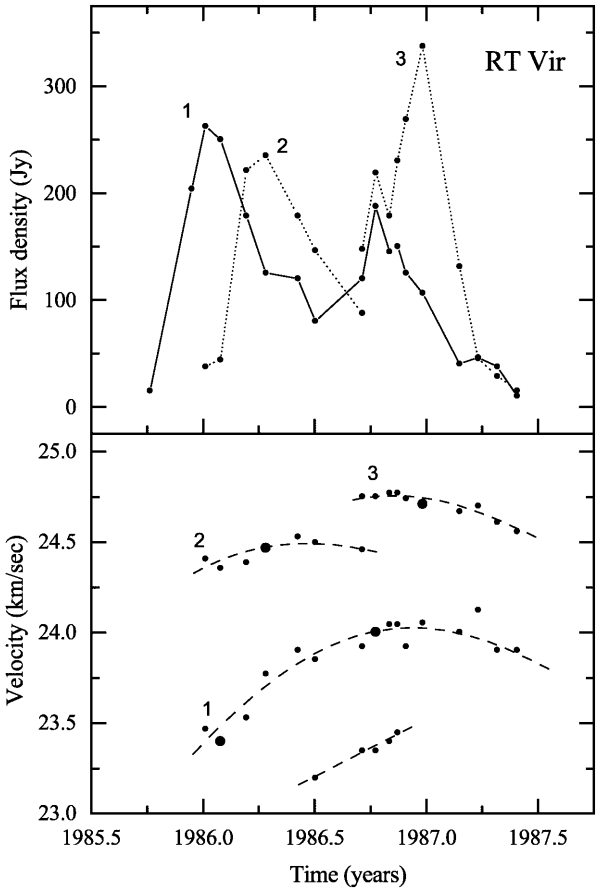

Fig. 7. Variability of the flux and radial velocity of the main features at $V_{\rm LSR} > 21$ km s^{-1} in 1985.8–1987.5. Big circles denote the velocities corresponding to the epochs of maximum flux.

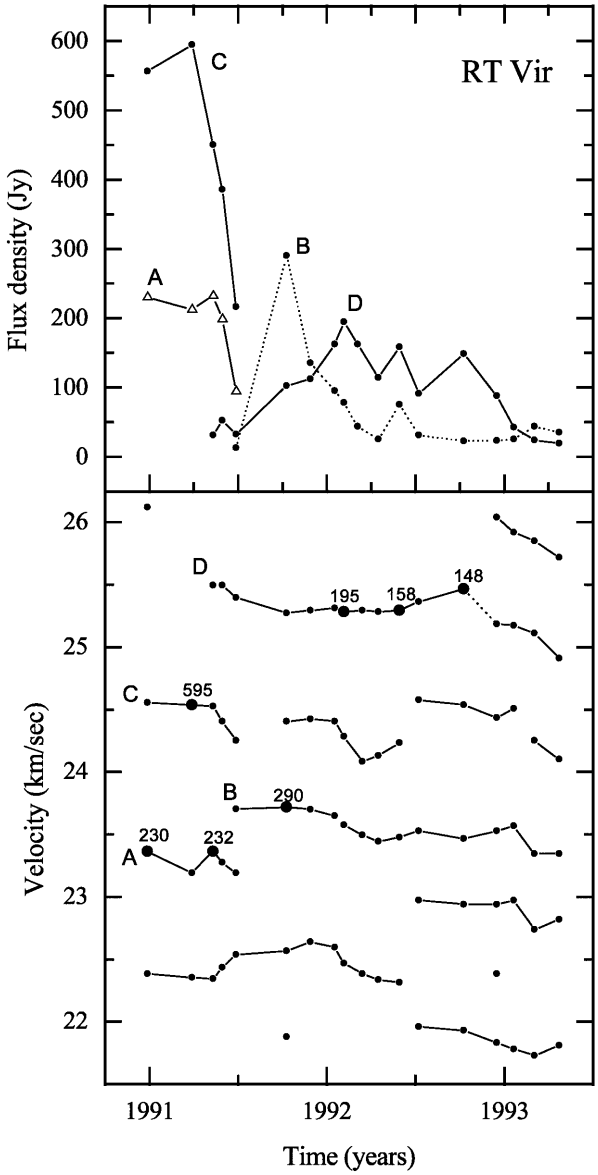

Fig. 8. Same as Fig. 7, but for 1991–1993.5. The numbers show the flux values at local maxima.

covered a long time interval in the evolution of the H_2O maser emission in RT Vir (more than 13 years), it is possible to use the superposition of the spectra and the mean spectrum to estimate the stellar velocity.

The superposition of all the spectra for 1984–1998 is shown in Fig. 10. At the beginning of 1985 and in mid-1998, strong flares happened at velocities of 12.6 and 11.2 km s^{-1}, respectively. In both cases, the peak flux density exceeded 2000 Jy. In order not to lose the clearness of the graph, the vertical scale was limited from above with a value of 840 Jy. For the same time interval, the mean spectrum was also calculated (Fig. 11).

4. Discussion

From Fig. 2 we see that during the entire timespan of our observations from 1984 to 1998 the H_2O maser emission of RT Vir has been strongly variable. We can represent the maser emission, drawn on a 3D plot, as a superposition of narrow emission peaks. The duration of a burst, measured at the half-maximum, is on the average about 0.5 yr. Each peak is not an individual spectral component; it just reflects one of the activity periods of the component. Some peaks are blends of components having similar radial velocities.

4.1. The structure of the H_2O spectrum and the stellar velocity

The limiting velocities in the H_2O spectrum were determined from the superposition of all the spectra and from the average spectrum. We adopted velocities as limiting, those from which the maser emission decreased to the noise level. We have obtained the following velocity interval: 8.3–26.3 km s^{-1} at a noise level of 10–15 Jy in the superposition of the spectra (Fig. 10) and 8.1–26.5 km s^{-1} at a level of 1–2 Jy in the average spectrum (Fig. 11). The average spectrum yields a broader velocity interval, however by only 0.2 km s^{-1} to each side. The essence of the difference consists in that in the average spectrum the noise level is considerably lower than in the superposition, and therefore weak emission in the average spectrum can be traced farther out at the edges.

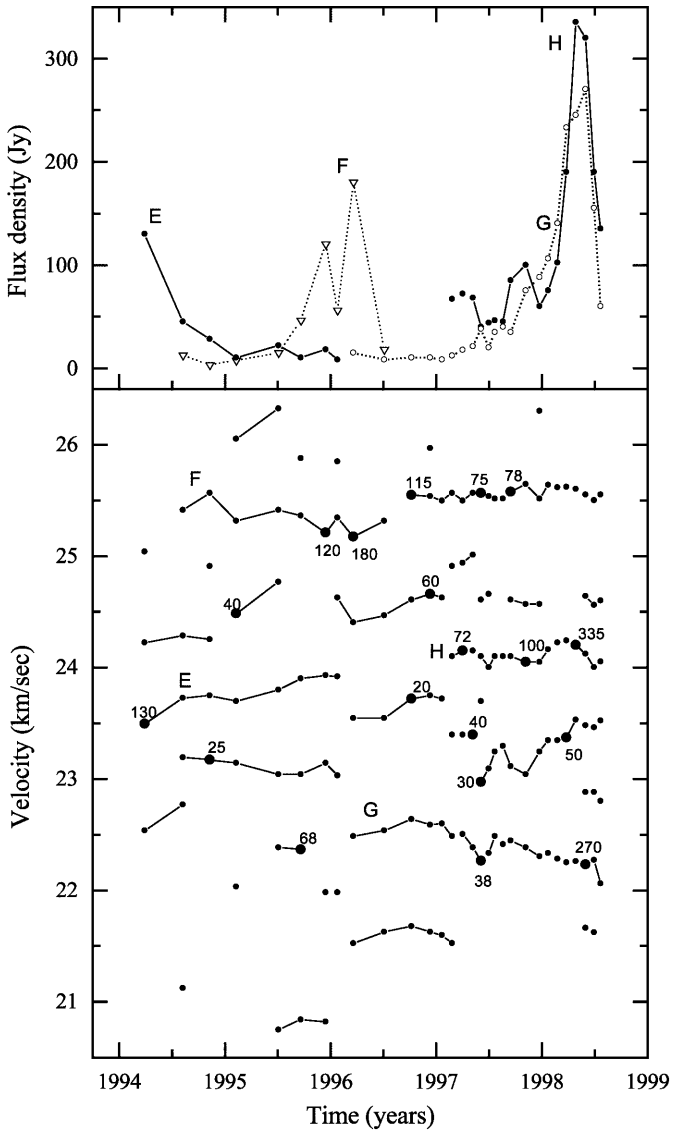

Fig. 9. Same as Fig. 7, but for 1994–1998.

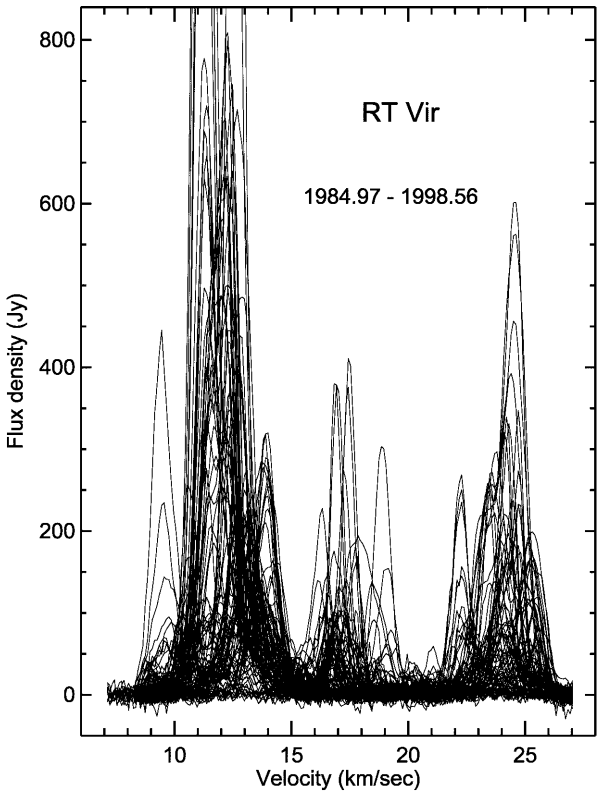

Fig. 10. Superposition of the H_2O spectra of RT Vir for 1986–1998.

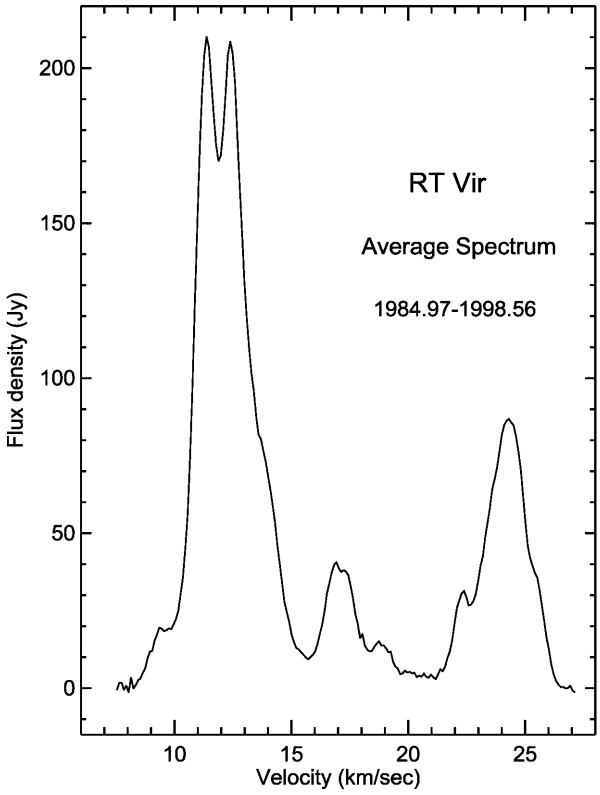

Fig. 11. The average spectrum of the H_2O maser emission of RT Vir for 1984–1998.

According to Fig. 10 and 11, the mean velocity of the emission and, according to our criteria (see Sect. 3.6), stellar velocity can be estimated as 17.3±0.2 km s^{-1}. This is close to V_* estimated from the OH spectra. We have observed the H_2O emission at a velocity interval of ±9.2 km s^{-1} with respect to the stellar velocity. There are prominent gaps of the emission down to 9 Jy near 15.3 km s^{-1} and to 4–5 Jy at velocities from 19.5 to 21.6 km s^{-1}. With respect to the stellar velocity we have estimated, these gaps lie near -2 km s^{-1} and in the interval of 2.2–4.3 km s^{-1}.

The gaps in the spectra indicate that not all the portions of the outflowing matter come to the zones of maser excitation. For the maser emission to arise, it is necessary to provide a combination of sufficient molecular abundance, velocity coherence and appropriate pumping conditions (Bowers & Johnston 1994). Apparently, for the existing structure of the envelope of RT Vir, some of the above–mentioned conditions are not fulfilled.

The gaps in the emission divide the entire spectrum into three segments. In the case of a strictly radial gas motion, the emission components of the blueshifted part ($V_{\rm LSR} < 15.5$ km s^{-1}) will have a component of the radial velocity with respect to the star that is directed toward the observer. The emission in this part of the spectrum is the most intense. The components of the redshifted part ($V_{\rm LSR} > 21$ km s^{-1}) have the opposite direction of motion. The emission of the central part is the weakest and rarely observable. The emission features in this region have doppler velocities close to the stellar velocity. However, they also display a radial–velocity drift (details will be given in a future publication). Probably they lie at small distances from the star and participate in both radial and tangential motions (Bowers et al. 1989; Bowers 1991). The tangential motion may arise from stellar rotation, viscosity in the anisotropic outflow or motion in the magnetic field.

4.2. The evolution of the features of the first group

For a more convenient analysis, we have presented the results of the observations of 1986–1998 in two figures: Fig. 3 (1986–1991) and Fig. 4 (1992–1998).

During 1986–1991 there were two local minima of the activity of this group of features (in mid-1986 and the beginning of 1990). At this time interval, all the components had a drift in radial velocity (an increase of the velocity with respect to stellar velocity V_*). The flux growth was slower than its decline. At that time the integral H_2O luminosity of the first group increased.

In 1990–1991 all the parameters became opposite in comparison to the first time interval. The drift direction reversed, i.e. the radial velocities of the features were decreasing with respect to V_*. The growth of the flux of the main feature 9 ($V \approx 13$–14 km s^{-1}) was faster, whereas the flux decrease was considerably slower. During 1992, there was a drift of the component in both directions. In 1990–1992 the integral flux of the group was decreasing.

The time interval of 1993–1998 was characterized by a transition of the H_2O maser RT Vir to its highest level of activity. The maser has been in its high state since mid-1996. From the beginning of the activity growth (1993) and till mid-1996, the velocity drift again was proceeding in only one direction (the doppler velocities of the features were decreasing).

From 1994–1998, features 12–14, 17 and 18 were the most intense. We see from Fig. 4 that features 12–14, like features 16–18, are separated by lacunas in the observations. During the second lacuna (in mid-1995), there was a minimum of the integral flux. Precisely at that time, considerable structural changes of the H_2O spectrum took place. Nevertheless, the existence of the preferential drift direction of the features allows us to speculate that there are two main chains of the features. In each of these chains, each subsequent feature is a continuation of the previous one. From what was said it follows that the group of features 15–18 can be identified with the same zone of maser excitation. The same can be said about features 11–14.

4.3. The evolution of the features of the third group

The H_2O maser emission of RT Vir at velocities above 21 km s^{-1} mainly took place at the time intervals of 1985.6–1987.3, 1990.5–1993.5 and since the end of 1993 till now. In the first two periods, a high maser activity was observed; it was accompanied by a decrease of the emission of the features of the first group, i.e., according to Mendoza-Torres et al. (1997) the fluxes of the first and third groups anticorrelated.

During the first interval (1985.6–1987.3), three most intense components were observed (Fig. 7); component 3 appeared immediately after the disappearance of component 2. Two consecutive maxima of the flux of component 1 (with an interval of 0.74 yr) are delayed in time with respect to the flux maxima of components 2 and 3 by 0.19 and 0.18 yr respectively, i.e. they have virtually the same delays. The velocity difference of components 2 and 1 was decreasing from 0.96 to 0.46 km s^{-1}, and that of components 3 and 1 remained practically constant at a level of 0.7 km s^{-1}. Only the direction of the drift of components 1 and 3 changed.

During the second and third intervals (since 1990.5), the spectra at velocities above 21 km s^{-1} were more extended in velocity and more complex. The number of features detected in spectra reached seven (Fig. 8 and 9). There was consecutive appearance of main features E, F and G–H (G and H coexisted simultaneously). Time intervals between maxima of their fluxes are approximately two years. In contrast to the features of the first group, in the third group there has not been any preferred direction of the radial–velocity drift since 1990.5, though the drift of individual features sometimes reached 0.4–0.5 km s^{-1} at a timescale of 1–2 yr. No correlation (or anticorrelation) was found between the variability of either fluxes of the features or their radial velocities.

4.4. The flare of the H_2O maser in 1998

In 1998, the flux of the majority of the features in the entire H_2O spectrum of RT Vir has increased. Interpolating the flux variability curves, we determined for these features the epochs of the maximum flux. For the features at 22.2 and 24.1 km s^{-1}, the maxima fall at epochs 1998.34 and 1998.37, respectively. The difference between the epochs is only 11 days. The major maximum of the main spectral peak at 11.25 km s^{-1} (epoch 1998.42) has a delay with respect to that of the feature at 24.1 km s^{-1} by another 18 days. The maximum of the main peak in the second group took place at epoch 1998.36. Thus, the maxima of all the main features of the H_2O are confined within one month on the time axis. The mean duration of the active phase of these features, measured at half-maximum flux, was 3.9 months. These figures are real, because in 1998 our observations were performed on a sufficiently regular basis: the minimum interval between two consecutive observational sessions was 22 days, maximum – 36 days, and mean – 29 days. The errors of the epochs of the maxima are within several days.

The uniqueness of the flare of 1998 is that a considerable increase of the fluxes of all the main components in the three

spectral groups took place within a short time interval (within one month). The strong flare of the H_2O maser RT Vir in 1985 was absolutely different. At that time, we observed consecutive appearance of individual components in the course of one year. According to Berulis et al. (1987), the flare of 1985 was caused by propagation of a shock wave, which consecutively excited different regions of the maser emission.

For the strongest feature of the flare of 1985 ($V_{\rm LSR}$ = 12.7 km s^{-1}, F = 2400 Jy at the peak), we found a functional relationship between the flux and linewidth (Berulis et al. 1987). In contrast to it, the flare of 1998 was characterized by amazing constancy of the linewidth: it varied only within the limits of 0.89–0.94 km s^{-1}. This scatter is most probably within the error limits. Another distinction is that the flare of 1985 took place against a much lower overall activity level of the maser RT Vir than the flare of 1998.

4.5. Variability of the radial velocities of the components

The radial velocities drift of the components was observed during all the time of the observations. Two types of the drift took place: the drift of most of the components predominantly in some one direction (most frequently corresponding to the increasing of component's velocity relative the star) and the drift of the components in both directions. For most of long–lived components (the life-time more than 3 years) the drift shows rather complicated trajectories. The maximum velocity variations of the components attained 1 km s^{-1} in a year. For intensive components the typical value of the velocity drift was about 0.5 km s^{-1} in a year. Maximum velocity variation of one component during its active phase was 1.5 km s^{-1}. The radial–velocity variations of the H_2O maser spectral components may be caused by anisotropic mass–loss.

We will present a detailed analysis of the variability of the maser emission for the components in the velocity interval of $15.5 < V_{\rm LSR} < 21$ km s^{-1} and linewidths of all the components in a forthcoming publication.

5. Conclusions

We have analyzed the spectra of the water-vapour maser RT Vir, obtained in 1986–1998. We separated the spectra into individual gaussian components. The time interval between consecutive observational sessions is mainly close to the timescale of intrinsic variations of the H_2O spectra of RT Vir. This enabled us to trace the evolution of multiple spectral components. An analysis of the flux, radial velocity and linewidth was done for the features from two main spectral groups ($V_{\rm LSR} < 15.5$ km s^{-1} and $V_{\rm LSR} > 21$ km s^{-1}). The main results are the following.

1. The H_2O maser emission of the semiregular variable RT Vir during 1984–1996 is well represented by a superposition of bursts of emission from individual spectral features (Fig. 2). The mean duration of the bursts is about 0.5 yr.
2. In March–June 1998, a strong flare of the maser took place. At that time there was a considerable growth of the flux density of multiple components of the H_2O spectrum. The flux density of the main component at a radial velocity of about 11.3 km s^{-1} reached 2025 Jy. In contrast to the flare of 1985, no functional relationship between the linewidth and flux density was present.
3. Using the superposition of all the spectra and the average spectrum, we have calculated the stellar velocity of RT Vir with respect to the Local Standard of Rest. Our estimate is 17.3±0.2 km s^{-1}.
4. The H_2O maser emission is observed in a velocity interval of ± 9.2 km s^{-1} with respect to stellar velocity V_*. The strongest emission is observed from -6 to -5.5 km s^{-1} and near 7 km s^{-1} with respect to V_*. Near -2 km s^{-1} and at the interval of 2.2–4.3 km s^{-1}, there are deep gaps in the H_2O emission spectra.
5. Virtually all the component displayed a radial–velocity drift. There were intervals with preferential direction of the drift. This effect was most pronounced for the components at $V_{\rm LSR} < 15.5$ km s^{-1}. The radial–velocity variations may be caused by anisotropic mass–loss.

Acknowledgements. The authors are grateful to the staff of the Pushchino Radio Astronomy Observatory, Lebedev Institute of Physics (Russia) for their help with the observations on the RT-22 radio telescope and to an anonymous referee for useful comments and advices, which allowed us to improve the article. This work was supported by the Russian Foundation for Basic Research (project code 96-02-18867), Russian Program of Integration of the High School and Science (grant No. 315), and Russian Federal Program in Astronomy and Fundamental Space Research (grant 1.4.3.1).

References

Berulis I.I., Lekht E.E., Pashchenko M.I., 1987, Pis'ma AZh 13, 305
Berulis I.I, Lekht E.E., Pashchenko M.I., 1994, Pis'ma AZh 20, 140
Bowers P.F., 1991, ApJS, 76, 1099
Bowers P.F., Claussen M.J., Johnston K.J., 1993, AJ 105, 284
Bowers P.F., Johnston K.J., 1994, ApJS 92, 189
Bowers P.F., Johnston K.J., de Vegt C., 1989, ApJ 340, 479
Collison A.J., Fix J.D., 1992, ApJ 390, 191
Le Squeren A.M., Baudry A., Brillet J., Darchy B., 1970, A&A 72, 72
Matveev L.T., 1976, Fundamentals of General Meteorology: Atmospheric Physics, Gidrometeoizdat, Leningrad, p. 480 (in Russian)
Mendoza–Torres J.E., Lekht E.E., Berulis I.I., Pashchenko M.I., 1997, A&AS 126, 257
Nyman L.-Å., Johansson L.E.B., Booth R.S., 1986, A&A 160, 352
Pascoli G., 1992, PASP 104, 350
Reid M.G., Menten K.M., 1990, ApJ 360, L51
Richards A.M.S., Yates J., Cohen R.J., Bains I., 1998, in: Asymptotic Giant Branch Stars, IAU Symp. No. 191, Montpellier (France), August 27 – September 1, 1998, Abstract Booklet, p. 140.
Spencer J.H., Johnston K.J., Moran J.M., Reid M.J., Walker R.C., 1981, ApJ 230, 449
Tseitlin N.M., 1976, Antenna Engineering and Radio Astronomy, Sovetskoe Radio, Moscow, p. 49 (in Russian)
Yates J.A., Cohen R.J., 1994, MNRAS 270, 958
Yates J.A., Cohen R.J., 1996, MNRAS 278, 655
Zhevakin S.A., Naumov A.P., 1963, Izvestia Vuzov, Radiofizika, 6, 674